Dynamical properties of the fossil group RX J1340.6+4018 [1]

Claudia L. Mendes de Oliveira
Departamento de Astronomia, Instituto de Astronomia, Geofísica e Ciências Atmosféricas da USP, Rua do Matão 1226, Cidade Universitária, 05508-090, São Paulo, Brazil
oliveira@astro.iag.usp.br

Eduardo S. Cypriano
Department of Physics & Astronomy, University College London, London, WC1E 6BT
esc@star.ucl.ac.uk

Renato A. Dupke
University of Michigan, Ann Arbor, MI 48109
rdupke@umich.edu

Laerte Sodré Jr.
Departamento de Astronomia, Instituto de Astronomia, Geofísica e Ciências Atmosféricas da USP, Rua do Matão 1226, Cidade Universitária, 05508-090, São Paulo, Brazil
laerte@astro.iag.usp.br

ABSTRACT

Fossil groups are systems with one single central elliptical galaxy and an unusual lack of luminous galaxies in the inner regions. Recent measurements of galaxy velocity dispersions and intragroup gas temperatures of these systems indicate that their characteristics are more consistent with those of poor clusters than of galaxy groups. In this study we show the results of an optical and X-ray analysis of RX J1340.6+4018, the prototype fossil group. Spectroscopy of 20 members shows that this system, at a mean redshift of 0.172, has a velocity dispersion of 565 km s^{-1}, a virial mass of $\sim 3.4 \times 10^{14}$ $M_\odot$, inside a radius of 516 h_{70}^{-1} kpc ($\sim 40\%$ R_{Vir}), a M/L of 347 $M_\odot/L_{g'\odot}$ and $L_{X(0.5-10keV)}$ of 2.3×10^{43} h_{50}^{-2} ergs s^{-1}. The luminosity function of RX J1340.6+4018, at the faint end, is similar to that of the Coma Cluster, displaying a sharp increase of low-luminosity galaxies, with a fit to the Schechter function parameter $\alpha = -1.6 \pm 0.2$, in both the g' and i' bands.

The standard explanation for the formation of fossil groups suggests that the lack of luminous galaxies in the inner regions is due to galactic cannibalism. Analysis of the SN Ia/SN II ejecta ratio in the inner and outrer regions shows a marginally significant central dominance of SN Ia material. This is consistent with what is found in other galaxy groups or cold clusters and it suggests that the lack of cooling cores in this group is unlikely to be due to secondary winds generated by galaxy merging involving late-type galaxies.

Subject headings: cosmology: observations – galaxies: clusters: individual: RXJ 1340.6+4018, RX J1552.2+2013, RX J1416.4+2315 – intergalactic medium — cooling flows — galaxies: elliptical and lenticular, cD – galaxies: evolution – galaxies: luminosity function, mass function – galaxies: kinematics and dynamics

1. Introduction

Fossil groups (FGs) are bright and extended X-ray emission systems ($L_{X,bol} > 10^{42}$ h_{50}^{-2} ergs s^{-1}) dominated by a single giant elliptical galaxy and with a two-magnitude difference between the first and second-ranked galaxies (in the R-band) within half of its virial radius. Initially, FGs were thought to be the cannibalistic remains of small galaxy groups that lost energy through tidal friction, perhaps the final stage of compact groups (e.g. Ponman and Bertram 1993, Jones et al. 2003). More recently, X-ray measurements of FGs were shown to be inconsistent with this formation mechanism, in particular because the intergalactic medium of a number of FGs is similar to those of galaxy clusters, with temperatures sometimes in excess of 4 keV (e.g. Khosroshahi et al. 2006; Khosroshahi et al 2007) and, thus, FGs have high gravitational masses compared with most nearby groups. As an example, one of the most massive Hickson compact groups known, HCG 62, is an order of magnitude less massive than the typical FGs studied so far (Mendes de Oliveira & Carrasco 2007).

The high masses of FGs estimated in X-rays were confirmed by the dynamical studies of these systems. Recent measurements of galaxy velocity dispersions in FGs (Mendes de Oliveira et al. 2006; Cypriano et al. 2006; Khosroshahi et al 2007) are fully consistent with the dynamical state of the system as determined from X-ray observations, indicating that they have relatively deep gravitational potential wells, typical of clusters.

The lack of L* galaxies in the central regions in a *cluster-sized* potential makes fossil groups quite intriguing objects. D'Onghia et al. (2005) and Dariush et al. (2007) suggested that these systems are older than clusters of comparable masses. Diaz et al. (2008, submitted) analyzed FGs in the millennium simulation (Springel et al. 2005) and in a mock catalogue and concluded that although FGs have assembled early, first-ranked galaxies in FGs only formed their magnitude gaps quite recently.

The most likely mechanism proposed for the lack of luminous galaxies surrounding the central dominant galaxy is cannibalism (e.g. Jones et al. 2003). The central merging, if not completely "dry" (i.e. involving gas-poor galaxies), should be accompanied by star formation bursts, causing subsequent metal rich SN II-driven galactic winds or superwinds (e.g. Sanders & Mirabel 1996). These secular winds would deposit metals and energy into the central gas and this extra energy may contribute to explain the typical lack of cooling cores in FGs (Sun et al. 2004; Khosroshahi et al 2004, 2007). The wind metal injection would make the central SN Ia/SN II ejecta of FGs different (lower) from that of normal groups and similar sized clusters. This scenario can, in principle, be tested by measuring individual elemental abundances and their ratios with sufficiently high S/N X-ray data (Dupke & Mendes de Oliveira 2008).

Based on the flat luminosity function of the fossil group RX J1340.6+4018 published by Jones et al. (2000) and on the conclusion that RX J1340.6+4018 lived in a sparse environment (Ponman et al. 1994), D'Onghia & Lake (2004) claimed that FGs may pose a severe problem for the cold dark matter models, since they did not have as much substructure as expected for such massive systems. On the other hand, Sales et al. (2007) using the millenium simulation found that the luminosity functions of three FGs, including RX J1340.6+4018, are not inconsistent with ΛCDM predictions, although the authors stress the current poor sample of FGs with reliable luminosity functions. New measurements and improvements in the determination of luminosity functions for these systems is of paramount importance to determine their origin. Here, we revise the luminosity function of the system RX J1340.6+4018, which is considered the prototype fossil group (Ponman et al. 1994).

In Section 2 we describe the optical and X-ray data we used in this work. In Section 3 we present the results we obtain using the optical data. In Section 4 the results obtained from the X-ray data are presented as well as the result of a test for the formation scenario of galaxies through canibalism of L* galaxies. Section 5 summarizes and discusses our findings. Throughout this paper, we adopt,

[1]Based on observations obtained at the Gemini Observatory, which is operated by the Association of Universities for Research in Astronomy, Inc., under a cooperative agreement with the NSF on behalf of the Gemini partnership: the National Science Foundation (United States), the Particle Physics and Astronomy Research Council (United Kingdom), the National Research Council (Canada), CONICYT (Chile), the Australian Research Council (Australia), CNPq (Brazil) and CONICET (Argentina) – Observing run ID: GN-2006B-Q-38.

unless explicitly mentionned otherwise, a cosmology with $H_0 = 70$ km s^{-1} Mpc^{-1}, $\Omega_0 = 0.3$ and $\Omega_\Lambda = 0.7$, so that $1'' \approx 2.9$ kpc at the cluster distance ($z = 0.172$, see Section 3.1).

2. Observations and Data Reduction

The imaging and multi-slit spectroscopic observations of the group RX J1340.6+4018 were done with the GMOS instrument, mounted on the Gemini North telescope, on May 2nd and June 22nd, in 2006, respectively (see sections 2.1 and 2.2 below). The X-ray study was based on archival Chandra data, as described in section 2.3.

2.1. Optical Imaging

The imaging consisted of 3 × 200s exposures in each of the two filters from the SDSS system (Fukugita et al. 1996) g′ and i′. The typical FWHM for point sources was ∼ 0.75" in all images. All observations were performed in photometric conditions. Fig. 1 displays the i′ image of the system.

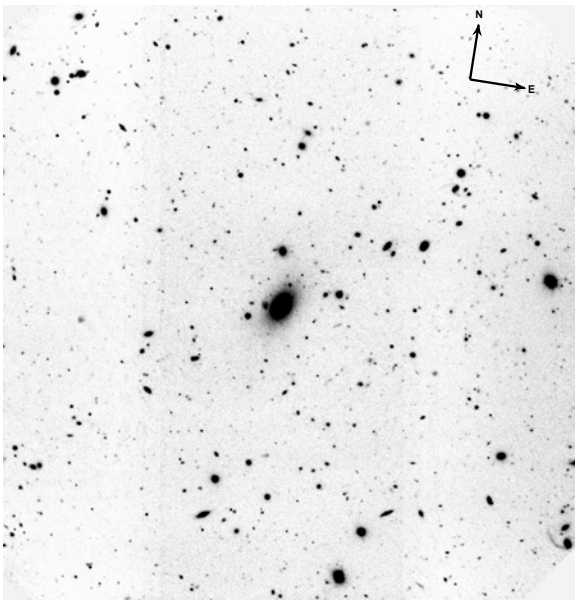

Fig. 1.— Optical i′ image of RX J1340.6+4018. The field of view is 5.6 arcmin on a side, or ∼ 980 h_{70}^{-1} kpc at the object redshift. The field orientation is shown in the upper right corner of the figure.

The calibration to the standard SDSS system was made using calibration stars observed about one month before the FG observations. No calibration stars were taken in the night of the FG observations, given that the telescope dome had to be closed due to strong winds shortly after the object observation. We confirmed the goodness of the i-band zero point obtained from the calibration stars by comparing magnitudes measured by us with those from the SDSS database, for 20 galaxies in common, in the magnitude range i=18-20, finding no systematic difference. All observations were processed in a standard way with the Gemini IRAF package v1.8 inside IRAF[1].

Positions and magnitudes (isophotal and aperture) were obtained for all objects. We estimate that the galaxy catalog is essentially complete down to 24.25 i′ magnitude (the peak of the number-count histogram). The SExtractor *stellarity* flag (Bertin and Arnouts 1996) was used to separate stars from galaxies. All objects with *stellarity* index ≤ 0.8 were selected as galaxies.

2.2. Optical Spectroscopy

Galaxies for spectroscopic follow-up were selected based in their magnitudes and colors. Figure 2 shows the color-magnitude diagrams for galaxies with $i' \leq 23.5$ mag. Objects in the region below the red cluster sequence (top line) and brighter than $i' = 22$ mag ($M_{i'} < -17.6$, vertical line) were selected as potential candidates. Galaxies above the red sequence are expected to be in the background, since their colors are redder than the expected colors of elliptical galaxies at the group redshift. The outermost galaxy, which turned out to be a member of the group/cluster, has a distance of 516 h_{70}^{-1} kpc from the X-ray center of RX J1340.6+4018 (which coincides very well with the central galaxy).

Four multi-slit exposures of 2400 seconds each was obtained through a mask with 1.0″ slits, using the R400 grating, for a final resolution of ∼8 Å (as measured from the FWHM of the arc lines), covering aproximately the range 4000 – 8000 Å (depending on the position of each slitlet).

Standard procedures were used to reduce the multi-slit spectra using tasks within the Gemini

[1]IRAF is distributed by NOAO, which is operated by the Association of Universities for Research in Astronomy Inc., under contract with the National Science Foundation

IRAF package. Wavelength calibration was done using Cu-Ar comparison-lamp exposures before and after the exposures.

Redshifts for galaxies with absorption lines were determined using the cross-correlation technique (Tonry & Davis 1979) as implemented in the package RVSAO (Kurtz & Mink 1998) running under IRAF. The final heliocentric velocities of the galaxies were obtained by cross-correlation with several template spectra. The final errors on the velocities were determined from the dispersion in the velocity estimates using several different galaxy and star templates. In the case of emission-line redshifts, errors were estimated from the dispersions in redshifts obtained using different emission lines. The S/N of the data, measured at the continuum region 6400–6500Å, ranged from 10 to 32.

Table 1 lists positions, isophotal magnitudes, aperture (g' - i') colors, radial velocities with errors and the Tonry & Davis cross-correlation coefficient R for all galaxies with reliable velocity determinations obtained in this study.

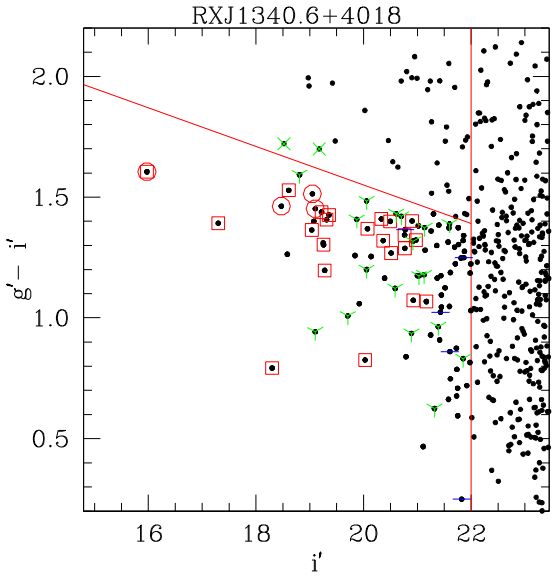

Fig. 2.— Color-magnitude diagram of the galaxies in the RX J1340.6+4018 field. Points marked with squares (members), 'Y' (non-members) and '–' (with spectra but no redshift) represent the galaxies observed spectroscopically by us with GMOS-N. The circles and 'X' represent, respectively, members and non-members published by Jones et al. (2000). The inclined line indicates the upper limit for the cluster red-sequence which we adopted when selecting the spectroscopic targets, whereas the vertical line is the limit in magnitude up to which we chose objects for spectroscopic follow up (i' = 22 mag).

TABLE 1

SPECTRAL DATA FOR GALAXIES IN THE FIELD OF RX J1340.6+4018

(1) Name [a]	(2) RA (2000)	(3) DEC (2000)	(4) i′ (AB Mag.)	(5) g′-i′	(6) cz (km s^{-1})	(7) R
G29.2+1704	13 40 29.2	40 17 04	20.98	1.32	50379 ± 41	4.1
G18.3+1830	13 40 18.3	40 18 30	19.26	1.30	50455 ± 137	7.0
G30.7+1539	13 40 30.7	40 15 39	18.61	1.53	50679 ± 41	7.2 [c]
G26.4+1811	13 40 26.4	40 18 11	20.76	1.34	50798 ± 57	2.6
G35.9+1826	13 40 35.9	40 18 26	20.33	1.41	50978 ± 39	5.0
G44.2+1902	13 40 44.2	40 19 02	20.36	1.32	51037 ± 60	3.0
G23.6+1817	13 40 23.6	40 18 17	19.31	1.41	51159 ± 48	4.6
G32.5+1612	13 40 32.5	40 16 12	19.36	1.43	51304 ± 46	6.0
G44.5+1637	13 40 44.5	40 16 37	19.04	1.36	51432 ± 100	3.0
G32.4+1533	13 40 32.4	40 15 33	20.77	1.29	51476 ± 38	5.6
G32.6+1910	13 40 32.6	40 19 10	19.22	1.44	51566 ± 30	7.8
G32.8+1740	13 40 32.8	40 17 40	15.46	1.60	51577 ± 39	8.9
G36.5+1843	13 40 36.5	40 18 43	20.50	1.40	51718 ± 64	4.0
G33.1+1753	13 40 33.1	40 17 53	20.90	1.40	51769 ± 84	2.4
G32.7+1934	13 40 32.7	40 19 34	20.92	1.07	51777 ± 64	3.0
G41.1+1558	13 40 41.1	40 15 58	20.07	1.37	51926 ± 37	6.2
G36.0+1604	13 40 36.0	40 16 04	20.51	1.27	52004 ± 36	5.9
G37.6+1517	13 40 37.6	40 15 17	17.30	1.39	52034 ± 32	7.2
G44.3+1612	13 40 44.3	40 16 12	19.28	1.20	52362 ± 18	... [b]
G40.4+1651	13 40 40.4	40 16 51	21.17	1.07	52412 ± 96	... [b]
G20.4+1918	13 40 20.4	40 19 18	20.03	0.83	52417 ± 52	6.8 [c]
G20.3+1924	13 40 20.3	40 19 24	18.30	0.79	52451 ± 27	8.1 [c]
G24.0+1618	13 40 24.0	40 16 18	20.92	1.32	58354 ± 85	2.7
G23.9+1904	13 40 23.9	40 19 04	20.06	1.48	60965 ± 39	6.6
G24.8+1953	13 40 24.8	40 19 53	20.89	0.93	61004 ± 137	... [b]
G40.4+1909	13 40 40.4	40 19 09	18.81	1.59	62707 ± 60	4.5
G18.3+1936	13 40 18.3	40 19 36	21.85	0.83	64905 ± 84	... [b]
G27.1+1642	13 40 27.1	40 16 42	19.71	1.01	66612 ± 44	6.7 [c]
G21.5+1930	13 40 21.5	40 19 30	19.11	0.94	85080 ± 56	4.5 [c]
G40.8+1841	13 40 40.8	40 18 41	20.06	1.20	90732 ± 53	... [b]
G34.4+1906	13 40 34.4	40 19 06	21.32	0.62	108043 ± 18	... [b]
G40.3+1900	13 40 40.3	40 19 00	19.87	1.41	119768 ± 32	... [b]
G19.5+1700	13 40 19.5	40 17 00	21.12	1.18	135990 ± 16	... [b]
G42.5+1705	13 40 42.5	40 17 05	21.60	1.39	145587 ± 39	... [b]
G21.8+1959	13 40 21.8	40 19 59	21.39	0.96	155841 ± 19	... [b]
G27.7+2013	13 40 27.7	40 20 13	20.59	1.12	156092 ± 30	... [b]
G19.9+1732	13 40 19.9	40 17 32	21.13	1.37	163895 ± 48	... [b]
G43.0+1701	13 40 43.0	40 17 01	21.03	1.17	181565 ± 54	... [b]
G26.6+1703	13 40 26.6	40 17 03	20.70	1.42	184426 ± 27	... [b]

2.3. X-rays

We analized *Chandra* archived data of the fossil group RX J1340.6+4018 in order to obtain its temperature and attempt a measurement of elemental abundance ratios. This system was observed by *Chandra* ACIS-S3 in Aug 2002 for 47.6 ksec. The cluster was centered on the S3 chip. The Ciao 3.3.0.1 with CALDB 3.2.4 was used, to screen the data. After correcting for a short flare-like period the resulting exposure time in our analysis was 46.3 ksec. A gain map correction was applied together with PHA and pixel randomization. ACIS particle background was cleaned as prescribed for VFAINT mode. Point sources were extracted and the background used in spectral fits was generated from blank-sky observations using the *acis_bkgrnd_lookup* script.

Here we show the results of spectral fittings with XSPEC V11.3.1 (Arnaud 1996) using the apec and Vapec thermal emission models. Metal abundances are measured relative to the solar photospheric values of Anders & Grevesse (1989). Galactic photoelectric absorption was incorporated using the wabs model (Morrison & McCammon 1983). Spectral channels were grouped to have at least 20 counts/channel. Energy ranges were restricted to 0.5–8.0 keV. The spectral fitting errors are 1-σ confidence unless stated otherwise. Given that individual abundances require a higher S/N than that observed in the outer regions, we tied Oxygen and Neon together since they have similar range of yield variation for SN Ia and II. Argon and Calcium are not well constrained and were also tied together in the spectral fittings. Fits with these elements untied did not produce significantly different results. For mass yields for SN Ia and SN II, we use the values of Nomoto et al. (1997a,b). SN II yields were calculated integrating over a Salpeter IMF for a progenitor mass range of 10 to 50 $M_{\odot}$.

3. Optical Properties of RX J1340.6+4018

3.1. Galaxy velocity distribution

Using the heliocentric radial velocities listed in Table 1, we consider as members of RX J1340.6+4018 the 22 galaxies with velocities between 50378 and 52451 km s^{-1}. The data were analyzed with the statistical software ROSTAT (Beers, Flynn & Gebhartd 1990), which did not find any large gap in the velocity distribution. In addition, no other data-points were found outside a $\pm 3\sigma$ range. Fig. 3 shows the velocity histogram for the 22 member galaxies studied by us.

Using the robust bi-weighted estimator, ROSTAT, the following values for the systemic redshift and velocity dispersion were found: $\langle z \rangle = 0.1720 \pm 0.0004$ and $\sigma = 565 \pm 77$ km s^{-1}, respectively. If we characterize the virial radius by the radius within which the interior density is 200 times of the critical density (r_{200}), the measured projected velocity dispersion implies a virial radius of $r_{200} = \sqrt{3}\ \sigma/10\ H(z) = 1.29 \pm 0.18\ Mpc$ (Carlberg et al. 1997). The errors cited are due only to the velocity dispersion determination and do not include the uncertainties implicit in the cited equation (such as departures from a $\rho \propto r^{-2}$ profile at large radii). This value is somewhat higher than that estimated from X-rays (see section 4), which can be given, as defined in Evrard, et al. (1996), by $r_{200} \sim 0.88\ \sqrt{(kT_{keV})} h_{70}^{-1}\ Mpc = 1.00 \pm 0.05\ Mpc$.

If the optically derived virial radius estimate is taken at face value, it would imply that RX J1340.6+4018 could not be classified "strictly" as a fossil group (in the Jones et al. definition) given that there is one galaxy, G37.6+1517, which is 1.8 magnitudes fainter than the brightest group galaxy in the i' band (1.6 in g'), and which is located at a clustercentric radius of 480kpc. We note that dos Santos et al. (2007) has also pointed out that RX J1340.6+4018 did not follow the strict definition of a fossil group.

We determine the dynamical mass of the system by using four different mass estimators, as suggested by Heisler et al. (1985): virial, projected, average and median mass estimators (see results on Table 2). The adopted center of mass of the system was the brightest cluster galaxy. The errors were calculated by using 1000 bootstrap simulations. Note that the dispersion between the mass values obtained using the several different methods is small compared to the errors in a single measurement. The average of the mass given by the four estimators is 3.4×10^{14} M$\odot$. We recall that all values are calculated within a radius of 516 h_{70}^{-1} kpc ($\sim$ 40% of the virial radius of the system).

TABLE 1—*Continued*

(1) Name [a]	(2) RA (2000)	(3) DEC (2000)	(4) i′ (AB Mag.)	(5) g′-i′	(6) cz (km s^{-1})	(7) R
G37.8+1818	13 40 37.8	40 18 18	20.61	1.43	191963 ± 27	··· [b]

[a]The names of the galaxies are based on their 2000 celestial coordinates (RA seconds and DEC minutes and seconds). Thus galaxy Gab.c+defg is located at 13 40 ab.c +40 de fg.

[b]Redshift measured from emission lines.

[c]Spectra with emission lines but with redshift measured from absorption lines.

TABLE 2
MASS ESTIMATES

(1) Estimator	(2) Mass (10^{14} $M_\odot$)	(3) $M/L_{g'\odot}$ ($M_\odot/L_{g'\odot}$)
Virial	3.23 ± 1.21	330
Projected	4.34 ± 1.42	443
Average	3.10 ± 1.05	316
Median	2.91 ± 1.36	297
Mean value	3.40	347

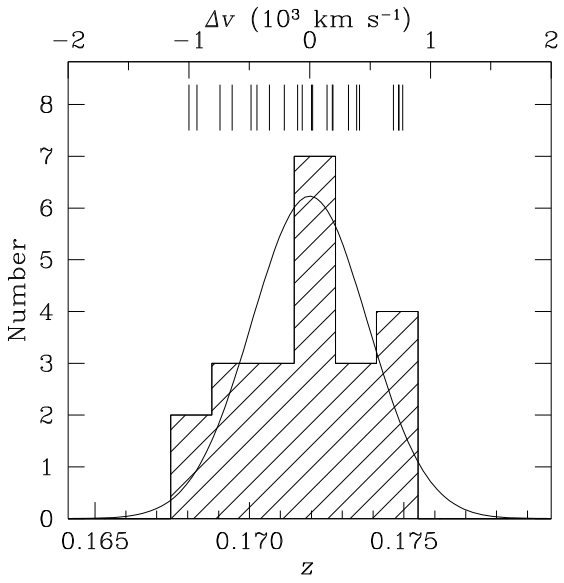

Fig. 3.— Velocity histogram of RX J1340.6+4018. It shows the distribution of the radial velocities of 22 galaxies in the inner 516 h_{70}^{-1} kpc radius, with redshifts within ±2000 km/s of the systemic velocity of the group. The sticks on the upper part of the plot show velocities of individual objects. The ROSAT bi-weighted estimator gives a velocity dispersion $\sigma = 565$ km/s and a redshift of $\langle z \rangle = 0.1720$, for the sample of 22 objects.

3.2. The Luminosity Function and Mass-to-Light Ratios

We show in Fig. 4 the luminosity function of RX J1340.6+4018 (solid circles) for galaxies with spectroscopically confirmed membership either obtained in this paper (22 galaxies) or given by Jones et al. (2003, three galaxies plus the central one, for the latter we also have a spectrum), corrected for incompleteness. The absolute magnitudes were calculated after correcting the observed magnitudes for Galactic extinction and applying k-corrections. The selection function (number of galaxies with reliable redshifts over the total number of galaxies in a given magnitude bin), also shown in Fig. 4, was calculated considering only galaxies bluer than the upper limit of the adopted red cluster sequence.

We have estimated the photometric luminosity function of RX J1340.6+4018 down to the completeness level of our photometric data ($g' = 24.75$ and $i' = 23.75$ mag) by adopting the procedure described in our previous papers (Mendes de Oliveira et al. 2006; Cypriano et al. 2006). The photometric luminosity functions are shown in Fig. 4 as open triangles. They go deeper than the spectroscopic results (solid circles) and they suggest that the number of galaxies keeps increasing at faint magnitudes. It is important to note that, at bright magnitudes, there is no important discrepancy between the luminosity functions calculated using both methods.

The shape of the luminosity function is very similar in the g' and i'-band diagrams. The faint end of the luminosity function is steeply rising up to our completeness limit. The shape of the photometric luminosity function in the i'-band, when fit to a Schechter function in the interval $-22.5 < M_{i'} < -16.5$, is well described by such a function with the following parameters: $M^*_{i'} = -21.3 \pm 1.8$ and $\alpha = -1.6 \pm 0.2$. For the g'-band, the photometric luminosity function is fit in the interval $-21.5 < M_{g'} < -15.5$, and the best fit to a Schechter function is given by the following parameters: $M^*_{g'} = -19.3 \pm 0.9$ and $\alpha = -1.6 \pm 0.2$. Lines indicating the best Schechter luminosity functions fitted are plotted in Fig. 4.

We integrated the best fit Schechter function on the g' band to obtain the total luminosity of the group, assuming that the magnitude of the Sun

in the g'-band is $M_{g'\odot} = 5.11$ mag [2]. We then added the luminosity of the central galaxy, since this galaxy is not taken into account when fitting the luminosity function. The final result is 9.8×10^{11} $L_{\odot}$on the g' band, where the central galaxy alone is responsible for almost 80% of the entire cluster luminosity budget. This leads to a mass-to-light ratio of 347 $M_{\odot}/L_{g'\odot}$ (using the mean value for the masses obtained with the four estimators, 3.4×10^{14} M$\odot$ - see Table 2). Results for the mass-to-light ratio, inside a radius of 516 h_{70}^{-1} kpc ($\sim 40\%$ R_{Vir}), using different mass estimators, are presented in Table 2.

3.3. Surface photometry of the BCG

In the upper panel of Fig. 5, the azimutally averaged photometric profile of the central galaxy of RX J1340.6+4018 is shown. The surface photometry was performed using the task ELLIPSE in STSDAS/IRAF, which fits ellipses to extended object isophotes. We allowed the ellipticity and position angle of the successive ellipses to change but the center remained fixed. The ellipse fitting was performed only in the deeper i′ image. For the g′-band image, the software measured the isophotal levels using the parameters estimated in the i′-band image. There are several small objects within the isophotes of the central galaxy which were masked during the profile fitting procedure.

We have fitted a $r^{1/4}$-law to the galaxy profile, from well outside the seeing disk (3.0″) to a radius corresponding to $\mu_{i'} = 24.0$ mag arcsec^{-2}. In the lower panel of Fig. 5, the residuals (data – $r^{1/4}$-law model) for the i′-band data are shown. There is no light excess over the de-Vaucoleurs profile indicating that this galaxy is not a cD.

4. X-ray properties of RX J1340.6+4018

4.1. ICM temperature and abundances

The gas temperature is consistent with a flat profile with a central (r<37″) value of 1.21±0.07 keV and outer value (112″ >r>37″) of 1.31±0.14 keV, consistent within the errors with the average value of 1.16±0.08 keV determined by Khosroshahi et al (2007). If a cold core is present, it is very mild and not seen with the current statistics. The iron abundance is consistent with a flat profile, but shows marginal signs of a central enhancement. Its central value is 0.29±0.09 Solar and in the outer regions we can only set an upper limit of 0.2 Solar. The measured value of the intracluster gas X-ray luminosity from 0.5–10 keV of RX J1340.6+4018 is $\sim 2.3 \times 10^{43}$ h_{50}^{-2} erg s^{-1}. According to the relations for groups and clusters from Mahdavi & Geller (2001), we find that for a system with this X-ray luminosity we would expect a velocity dispersion of about $\sigma = 425$ km s^{-1}, in good agreement with our direct measurement, given the high scattering in the L_X–σ relation (±240 km/s).

4.2. Central abundance ratios and fossil group formation models

The isolation of the central galaxy in FGs and the correlation between the FG's X-ray and central galaxy's optical luminosities suggest that the formation process of these systems involve the merging of central bright galaxies due to dynamical friction. Given the time scales for dynamical friction, it was originally suggested that FGs have an earlier formation epoch than regular groups (e.g. Ponman et al. 1994). This is also in agreement with predictions of the concentration parameters and magnitude differences of the two brightest galaxies in FGs from numerical simulations (Wechsler et al. 2002, Donghia et al. 2005). However, the cooling time of FGs is observed to be significantly below the Hubble time (e.g., RX J1416.4+2315, ESO 3060170, Sun et al. (2004); NGC 6482, Khosroshahi et al. (2004, 2006), but they typically *lack cooling cores*, in disagreement with what one would expect for an old undisturbed system. This is a notable difference from regular rich groups, which often show cooling cores (e.g. Finoguenov & Ponman 1999), even in spite of strong AGN activity.

To try to solve this apparent contradiction it is desirable to have other independent formation age indicators. Elemental abundances measured in the central regions of FGs can be used as such (Dupke, Mendes de Oliveira & Sodre 2008). The general idea is based on the fact that different metal enrichment mechanisms contaminate the intragroup medium with different relative ejecta dominance and are more intense at differ-

[2]Calculated by C. Willmer using the solar spectra: www.ucolick.org/∼cnaw/sun.html

ent cluster locations and in different time scales. For example, protogalactic winds are dominated mostly by SN II and produce an early more distributed background of SN II ejecta throughout the group/cluster, while ram-pressure stripping happens continuously throughout the cluster's history and creates a more concentrated SN Ia contamination, given its dependence on the ambient density.

If the group has an earlier origin and has been undisturbed for a long time, the above mentioned enrichment processes will develop a radial chemical gradient in such a way as to increase the central Fe mass fraction dominance from SN Ia, which is observed in rich groups and clusters of galaxies (e.g. Dupke 1999; Dupke & White 2000a,b; Allen et al 2001; Finoguenov et al. 2000; Dupke & Arnaud 2001); If the mergers are "dry", i.e., involving gasless galaxies, an older system should have a higher SN Ia central enhancement than a younger system. This central SN Ia enhancement has not been observed yet in any FG. In fact, most FGs seem to have an inverted trend of reduced central SN Ia dominance (Dupke, Mendes de Oliveira, & Sodre 2008), suggesting that, without fine tuning, the difference between FGs and regular groups is not due to age but to the type of merger that created the central galaxy. Gas rich galaxy mergers presumably would be accompanied by SN II powered winds, diluting the SN Ia central dominance.

In order to compare the enrichment distribution, we selected two regions for spectral analysis. The first corresponds to the typical cooling radius, where the cooling time is less than the Hubble time (assumed as $\sim$ 100kpc or 10% of r_{200}, which is determined according to $r_{200} \sim 0.88\sqrt{(kT_{keV})}h_{70}^{-1}$ Mpc) and is denoted r_{cool}. The second region is an annulus going from the border of r_{cool} to $\sim$ 320 kpc, denominated outer in Table 3. A central circular region with 5 kpc radius was excluded to account for possible AGN contamination. Even though the current observation does not allow us to determine variations of the abundance of different α-elements significantly, there seems to be an overall tendency for the abundance of the α–elements silicon, sulfur, oxygen and magnesium to decline towards the central regions. The results are shown in Table 3 and suggest a gradient in the supernovae type enrichment dominance, unlike that of other FGs (Dupke, Mendes de Oliveira & Sodre 2008), but similar to that found in rich groups and poor clusters. The number of counts is very small for the analysis of individual ratios, so that we can only analyze an ensemble of abundance ratios. The error weighted average of the abundance ratios O/Fe, Si/Fe, S/Fe and Mg/Fe indicates that the SN Ia Fe mass fraction in the central regions of RX J1340.6+4018 is 91$\pm$9% declining to $\sim$0% in the outer parts.

TABLE 3
INDIVIDUAL ELEMENTAL ABUNDANCE PROFILES[a]

Element	Inner r_{cool}[b]	Outer[b]
O	$0.0^{+0.15}{}_{-0.0}$[c]	$0.4^{+2.0}_{-0.40}$
Mg	$0.41^{+0.46}_{-0.36}$	$1.55^{+1.95}_{-0.85}$
Si	$0.26^{+0.29}_{-0.22}$	$0.44^{+0.96}_{-0.34}$
S	$0.0^{+0.26}_{-0.0}$	$1.78^{+3.72}_{-1.78}$
Fe	$0.29^{+0.10}_{-0.09}$	$0.0^{+0.2}_{-0.0}$

[a]Abundances are measured relative to the solar photospheric values of Anders & Grevesse (1989), in which Fe/H = 4.68×10^{-5} by number

[b]χ^2_ν for the spectral fittings are 1.16 and 1.52 for 39 and 110 D.O.F. for the inner and outer regions respectively

[c]Errors are 68% confidence limits

5. Discussion

Here we summarize our main findings in this optical and X-ray study of RX J1340.6+4018:

- RX J1340.6+4018 is a cluster-like fossil group at $z = 0.172$, with a velocity dispersion of 565 km/s and a mass of $\sim$3.4 $\times$ 10^{14} $M_{\odot}$within 516 h_{70}^{-1} kpc (about 40% of its virial radius). Thus, the prototype FG is indeed a cluster, not a group.

- We find a steep faint-end for the galaxy luminosity function of the cluster (with α = –1.6), in disagreement with the flat luminosity function previously reported by Jones et al. (2000). The originally reported flat luminosity function caused D'Onghia et al. (2005) to propose that FGs would also be affected by the missing satellite problem of groups with masses comparable to our Local Group. The results of this paper indicate that this problem does not exist any longer, for RX J1340.6+4018.

- The brightest object of RX J1340.6+4018 is not a cD galaxy. Its surface brightness profile follows a de Vaucouleurs-law out to 2.5 effective radii.

- The X-ray analysis of the elemental abundance ratio profiles indicates that the Fe mass fraction in the central region is dominated by SN Ia contamination, similar to other groups and poor clusters of galaxies. This suggests that either the merger which originated the central galaxy was "dry" (the galaxies involved in this process were gas poor), or the group has been formed at early epochs.

- RX J1340.6+4018 does not constitute a low-density environment. Like RX J1552.2+2013 and RX J1416.4+2315, this object is a galaxy cluster with a large magnitude gap in the bright end. The fairly high X-ray emission, the large fraction of elliptical galaxies (most of the bright galaxies in Fig. 1 are early-types), the radial velocity distribution (Fig. 3), as well as the lack of obvious substructures, imply a high degree of virialization for RX J1340.6+4018.

Fossil groups have, by definition, a lack of bright galaxies because of the selection criteria used to catalogue them. The bright-end of the luminosity function of these systems is then known to be unusual, with too few L^* galaxies. At the faint-end, not much has been known so far, but a scenario seems to be emerging that the massive FGs have steep luminosity functions with exception of perhaps RX J1552.2+2013, for which we just reach the magnitude of the dwarf upturn (the point where the curve goes from being giant-dominated to dwarf-dominated). For the particular case studied here, of RX J1340.6+4018, the faint end of its luminosity function is similar to that of other galaxy clusters of comparable masses. For an example, for the 2dF and RASS–SDSS clusters, $\alpha \simeq -1.3$ in the blue-band (de Propris et al. 2003; Popesso et al. 2005). It is also comparable with the faint-end slope of the Coma cluster.

We found that RX J1340.6+4018 does not show any light excess over its de Vaucouleurs profile (which would characterize a cD galaxy). So far, only one central galaxy of a FG, that of RX J1552.2+2013, has been classified as a cD (perhaps not coincidentally, it is also the only FG observed to have a declining luminosity function at $\sim M^* + 4$).

The best accepted scenario for the formation of FGs involves the merging of the central bright galaxies. The lack of SN II ejecta dominance in the central regions of RX J1340.6+4018 implies that the mergers that formed the central galaxy were "dry". The overall results are consistent with an early epoch origin for this FG, so that it has been undisturbed for a long time and central replenishment with SN Ia material, through e.g., ram-pressure stripping, has not been affected by secondary SN II winds. The lack of a cooling core in this system is, therefore, still an open question. The scenario of fossil group formation may become clearer when more of these groups are studied spectroscopically. Ongoing determinations of the luminosity function for a large sample of fossil groups and the detailed study of the properties of the brightest group members, including the determination of their ages and metal abundances, may also elucidate some of the unsolved problems regarding these systems.

We are grateful to H. Khosroshahi for communicating velocities for three members of the group, which were used in the determination of the spectroscopic luminosity function. We thank Raimundo Lopes de Oliveira for a careful reading of the manuscript and useful suggestions. We would also like to thank the Gemini staff for obtaining the observations. The authors would like to acknowledge support from the Brazilian agencies FAPESP (projeto temático 01/07342-7), CNPq and CAPES. Dupke also acknowledges support from NASA Grants NAG 5-3247, NNG05GQ11, GO4-5145X, GO5-6139X & FAPESP grant 06/05787-5. We made use of the Hyperleda database and the NASA/IPAC Extragalactic Database (NED). The latter is operated by the Jet Propulsion Laboratory, California Institute of Technology, under contract with NASA.

REFERENCES

Allen, S. W., Fabian, A. C., Johnstone, R. M., Arnaud, K. A., & Nulsen, P. E. J., 2001, MNRAS, 322, 589

Baumgartner, W. H., Loewenstein, M., Horner, D. J., & Mushotzky, R. F., 2005, ApJ, 620, 680

Beers, T. C., Flynn K. & Gebhardt 1990, AJ, 100, 32

Bertin, E. & Arnouts, S. 1996, A&AS, 117, 393

Carlberg, R. G., Yee,H. K. C., & Ellingson, E. 1997, ApJ, 478, 462

Cypriano, E. S., Mendes de Oliveira, C. L. & Sodré Jr., L. 2006, AJ, 132, 514

Dariush, A., Khosroshahi, H. G., Ponman, T. J., Pearce, F., Raychaudhury, S., & Hartley, W. 2007, MNRAS, 962

D'Onghia, E., Lake, G. 2004, ApJ, 612, 628

D'Onghia, E., Sommer-Larsen, J., Romeo, A. D., Burkert, A., Pedersen, K., Portinari, L., & Rasmussen, J. 2005, ApJ, 630, L109

dos Santos, W., Mendes de Oliveira, C., Sodré Jr., L. 2007, AJ, 134, 155

Dupke, R. A., 1998, PhD Thesis, University of Alabama

Dupke, R. A. & Arnaud, K. 2001, ApJ, 548, 141

Dupke, R. A. & White, R. E. III 2000a, ApJ, 537, 123

Dupke, R. A. & White, R. E. III 2000b, ApJ, 528, 139

Dupke, R. A., & Mendes de Oliveira, C. 2008, ApJ, to be submitted

Evrard, A. E., Metzler, C. A., & Navarro, J. F. 1996, ApJ 469, 494

Finoguenov et al. 2000, ApJ544, 188

Fukazawa, Y., Makishima, K., Tamura, T., Ezawa, H., Xu, H., Ikebe, Y., Kikuchi, K., & Ohashi, T. 1998, PASJ 50, 187 Ichikawa(1995)]fukugita95 Fukugita, M., T. 1995, PASP, 107, 945

Fukugita, M., Ichikawa, T., Gunn, J. E., Doi, M., Shimasaku, K. & Schneider, D. P. 1996, AJ, 111, 1748

Girardi, M. & Mezzeti, M. 2001, ApJ, 548, 79

Heisler, J.. Tremaine, S.. Bahcall, J. N. 1985, ApJ, 298, 8

Hook, Isobel, Allington-Smith, J. R., Beard, S. et al. 2002, SPIE, 4841, Power Telescopes and Instrumentation into the New Millennium

Heckman, T. M., Armus, L., & Miley, G. K. 1990, ApJS, 74, 833

Jones, L. R., Ponman, T. J., Forbes, Duncan A. 2000, MNRAS, 312, 139

Jones, L. R., Ponman, T. J., Horton, A., Babul, A., Ebeling, H., Burke, D. J. 2003, MNRAS, 343, 627

Khochfar, S. & Burkett, A. 2005, MNRAS, 359, 1379

Khosroshahi, Habib G., Jones, Laurence R., Ponman, Trevor J. 2004, MNRAS, 349, 1240

Khosroshahi, H. G., Maughan, B. J., Ponman, T. J., & Jones, L. R. 2006, MNRAS, 369, 1211

Khosroshahi, Habib G., Ponman, Trevor J., & Jones, Laurence R., 2006, MNRAS, 372, L68

Khosroshahi, Habib G., Ponman, Trevor J., & Jones, Laurence R., 2007, MNRAS, 377, 595

Kurtz, M. J. & Mink, D. J. 1998, PASP, 110

Mahdavi, A., Geller, M.J. 2001, ApJ, 554, 129

Mendes de Oliveira, C. L., Cypriano, E. S., Sodré Jr., L. 2006, AJ, 131, 158

Mendes de Oliveira, C. L., & Carrasco, E. R. 2007, ApJ, 670, L93

Mushotzky, R., Loewenstein, M., Arnaud, K. A., Tamura, T., Fukazawa, Y., Matsushita, K., Kikuchi, K., & Hatsukade, I. ApJ, 466, 686

Ponman, T. J., Allan, D. J., Jones, L. R., Merrifield, M., McHardy, I. M., Lehto, H. J., Luppino, G. A. 1994, Nature, 369, 462

Popesso, P., Böhringer, H., Romaniello, M., Voges, W. 2005, A&A, 433, 415

De Propris, R. et al. 2003, MNRAS, 342, 725

Sales, L. V., Navarro, J. F., Lambas, D. G., White, S. D. M., & Croton, D. J. 2007, MNRAS (accepted; arXiv:0706.2009)

Sanders, D. B. & Mirabel, I. F. 1996, ARA&A, 34, 749

Schlegel, S., Finkbeiner, D. P. & Davies, M. 1998, ApJ, 500, 525

Springel, V., et al. 2005, Nature, 435, 629

Sun, M., Forman, W., Vikhlinin, A., Hornstrup, A., Jones, C., Murray, S. S. 2004, ApJ, 612, 805

Tonry, J. & Davis, M. 1979, AJ, 84, 1511

This 2-column preprint was prepared with the AAS LaTeX macros v5.2.

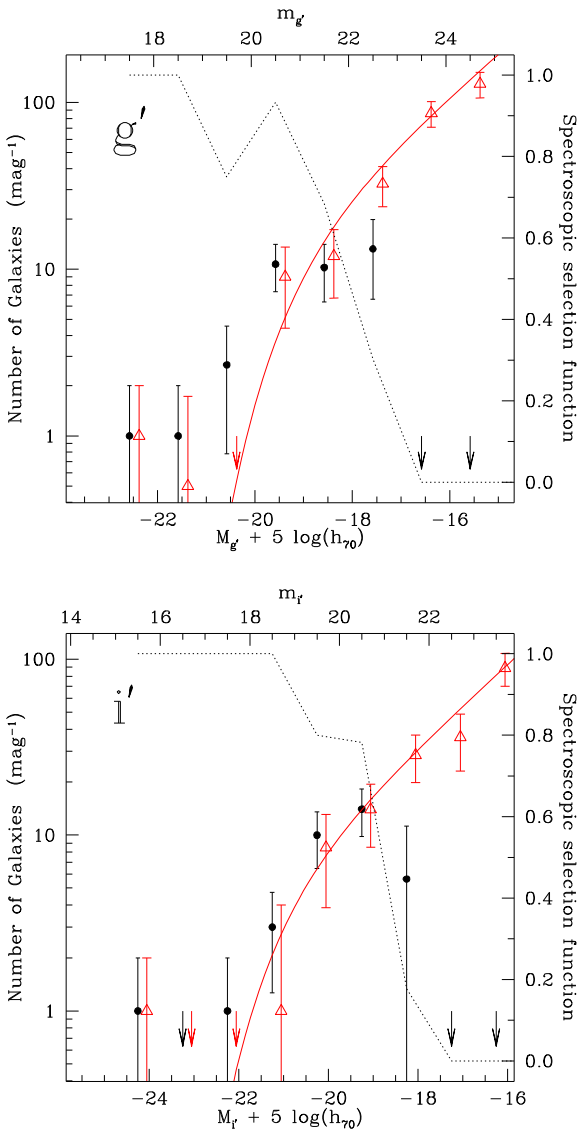

Fig. 4.— Luminosity functions of RX J1340.6+4018 in the g′ and i′ bands. The solid circles show the completeness-corrected numbers of spectroscopically confirmed members of RX J1340.6+4018 per 1.0 magnitude bin in the GMOS field. The error bars are 1σ Poissonian errors. The arrows show bins with number of galaxies less or equal to zero. The dotted line is the selection function of the spectroscopic sample. The open triangles show the photometrically-determined luminosity function estimated through number counts and statistical subtraction of the background. The points have been shifted by 0.2 mag (from the center of the bin), for the sake of clarity. The continuous lines show the best fitted Schechter function of the photometric sample. The brightest galaxy of the cluster was not included in the fit. The agreement between the spectroscopically and photometrically-determined luminosity functions

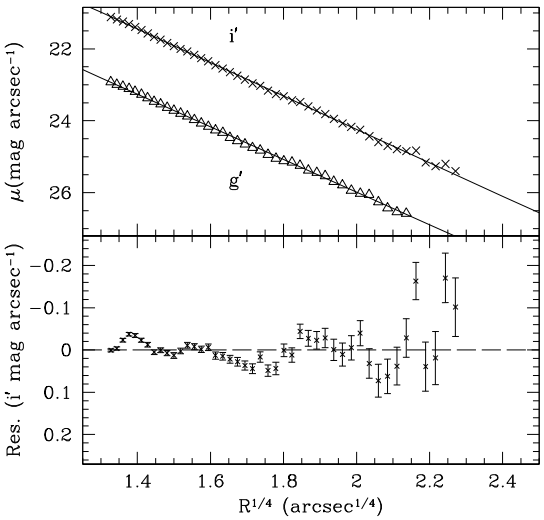

Fig. 5.— *Upper panel:* Photometric profile of the central galaxy of RX J1340.6+4018. We show the isophotal levels as a function of the semi-major axis to the power 1/4. The solid line is the best fit to the de Vaucoleurs profile in the region where r>3.0arcsec and $\mu_{i'} = 25.0$ mag arcsec^{-2}. *Lower panel:* residual between the actual r′-band profile and the de Vaucoleurs profile fit.